Bull. Mater. Sci. (2023) 46:234
https://doi.org/10.1007/s12034-023-03076-1

The effect of the Y_2O_3 buffer layer on the microstructural and physical properties of melt-processed Y358 superconductor

MEHMET BAŞOĞLU[1,*], BAKIYE ÇAKIR[2], ŞEYDA DUMAN[2] and ALEV AYDINER[3]

[1]Department of Electric and Energy, Gümüşhane Vocational School, Gümüşhane University, 29100 Gümüşhane, Turkey
[2]Department of Medical Services and Techniques, Vocational School of Health Services, Artvin Çoruh University, 08000 Artvin, Turkey
[3]Department of Physics, Faculty of Sciences, Karadeniz Technical University, 61080 Trabzon, Turkey
*Author for correspondence (mehmetbasoglu@gumushane.edu.tr)

MS received 26 May 2023; accepted 10 September 2023

Abstract. The $Y_3Ba_5Cu_8O_{18}$ (Y358) superconductors were produced using the Melt-Powder-Melt-Growth (MPMG) method. In the crystal growth process, Y_2O_3 powder was used as a substrate in both powder and tablet form. The first sample was produced without using any buffer layer, the second sample was produced with a powdered Y_2O_3 buffer layer, and the third sample was produced with a tablet-form Y_2O_3 buffer layer. The effect of the Y_2O_3 substrate on the structural and physical properties of the Y358 superconductor samples was investigated. Superconducting phases were observed in all samples of Y358 through XRD measurements, confirming their presence. Samples fabricated using the powder and tablet forms of the Y_2O_3 substrate had a better microstructure than the sample fabricated without a Y_2O_3 substrate. The highest critical current density (J_c) value was obtained at 77 K for the Y358 sample produced with a Y_2O_3 powder substrate, and the J_c value was calculated as 1.2×10^4 A cm^{-2} according to the Bean model.

Keywords. MPMG Y358; Y_2O_3 buffer layer; activation energy; critical current density.

1. Introduction

The levitation force is the weight the bulk superconductor can carry and the trapped field capacity is the maximum field the bulk superconductor can produce. These two main material properties are required for industrial applications [1]. Y–Ba–Cu–O (YBCO) and Re–Ba–Cu–O (Re: Nd, Sm, Eu, Gd, Dy, Ho, Er, Tm, Yb, Lu, La) bulk superconductors are used to obtain high magnetization [2–4]. These superconductors show strong bulk magnetic properties at liquid nitrogen temperature and are also suitable for obtaining large-grained superconductors with a suitable fabrication method. It is known that the field trapping ability of large single-grain bulk superconductors is superior to that of conventional permanent magnets [1,5]. The bulk superconducting magnet can generate a larger field with increasing critical current density (J_c) and volume. Large-grained YBCO and Re–Ba–Cu–O superconducting samples with a diameter of $\approx$10 cm can be obtained by melting methods [1]. Superconductors can trap a magnetic field of 1.5 T at 77 K and 17 T at 29 K [6].

The trapped field is proportional to the diameter of the sample, and the grain size must be increased to improve the performance of bulk superconductors. However, since the total flux will increase, increasing the grain size for technological applications is important. Since the J_c is directly related to the performance of the superconductor, single-grain materials aligned in the c-axis must be grown to obtain high J_c. For this reason, many melting methods have been developed [7].

Bulk superconducting samples fabricated by melting methods give more effective results than the samples fabricated by solid-state reaction methods [8]. Melt-processed $YBa_2Cu_3O_7$ (Y123) superconductors have the potential to be used in many applications, such as magnetic beds, flywheel energy storage systems, magnets and magnetic rail trains (MAGLEV) [9–11]. It was reported that the $Y_3Ba_5Cu_8O_{18}$ (Y358) superconductor, which was produced using the solid-state reaction method in 2009 and the melting method in 2012, has a higher transition temperature than the Y123 superconductor [12,13]. Y358 superconductors have a perovskite structure and are tetragonal or orthorhombic depending on the amount of oxygen in their structure, like the other phases of the Y123 family. The a, b lattice parameters of the unit cell of Y358 are close to those of the Y123 superconductor, and the c parameter is about three times higher. Although it has been reported that the transition temperature is around 110 K, it is not certain whether the transition temperature of this phase is different from the traditional Y123 phase [12–15].

In previous studies, the use of a Y_2O_3 layer in the growth of Y123 produced by the Melt-Powder-Melt-Growth

Published online: 09 December 2023

(MPMG) method was investigated. It was observed that the Y_2O_3 substrate, which was used in two different ways as powder and tablet, had supportive effects on sample growth [16,17]. Since Y123 and Y358 superconductors have similar structures, this study was aimed to investigate the effects of the Y_2O_3 layer on the growth of Y358 bulks. In this context, the Y358 sample was produced using the MPMG method. A total of three samples were produced. The first sample was produced with no substrate placed under the sample, which was pressed into tablet form. The second sample was produced by using a powdered Y_2O_3 substrate, and the third sample was produced by using a tablet Y_2O_3 substrate. The effect of the Y_2O_3 layer on the microstructural and physical properties of the produced Y358 samples were investigated.

2. Experimental

Superconducting samples were produced using the Melt-Powder-Melt-Growth (MPMG) method. Y_2O_3, $BaCO_3$ and CuO are weighed appropriately to obtain $Y_3Ba_5Cu_8O_{18}$ (Y358) superconducting samples. The weighed powders were mixed manually in the grinding bowl for 15 min and then ground in the grinding machine for 1 h. The ground powdered mixture placed in the Al_2O_3 crucible was calcined at 880°C for 24 h in a square furnace with intermediate grinding. After the calcination process, the ground powders were placed in a platinum crucible, melted at 1450°C and poured onto a copper plate, and then the melted powders were cooled quickly by hitting it with another copper plate. The molten material obtained after rapid cooling was ground again for 1 h, and starting powders were obtained. The preparation of the starting powders is described in detail in reference [15]. The starting powders of 12 g were weighed and placed in a mould with a diameter of 20 mm and formed into a cylindrical pellet by applying 300 MPa pressure. While placing the pellet samples on the Al_2O_3 crucible, no substrate was placed below the Y358-a sample, a powder form of Y_2O_3 was placed below the Y358-b sample, and a 30 mm diameter 1 mm Y_2O_3 tablet was placed below the Y358-c (figure 1). The crystal growth process was carried out by applying the heat treatment which is shown in figure 2 for the pellets placed on the Al_2O_3 crucible. The fabricated samples were annealed at 450°C with 150 ml min^{-1} and flow rate for 200 h in an oxygen environment.

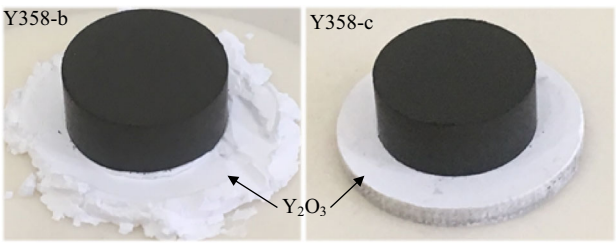

Figure 1. Placement of the Y_2O_3 substrate in powder and tablet form under the samples during production.

Differential thermal analysis (DTA) was performed on the melted powder to determine its peritectic decomposition temperature on heating. The crystal structures of the samples were characterized through X-ray diffraction measurements using a Rikagu D/Max III C diffractometer with Cu Kα radiation (λ = 1.5418 Å, 40 kV, 30 mA), within the 2θ range of 20° to 60°. Polarized light optical microscope was used to take optical micrographs. Scanning electron microscope (SEM) images were taken to examine the surface morphology of the produced samples.

Low-temperature resistivity measurement was performed by the standard four-probe method in the *ab*-plane using a Quantum Design Physical Properties Measurement System (PPMS) under the different magnitudes of the applied magnetic field between 0 and 3 T. The samples were cooled in the zero-field cooling regime, and the field was applied parallel to the *c*-axis. The magnetization (M-H) measurements were calculated by using a vibrating sample magnetometer (VSM) module of the PPMS system at constant temperatures of 20 and 77 K, at a sweep speed of 200 Oe s^{-1}, and by applying a magnetic field between –50000 and +50000 Oe. Prior to each measurement, the samples were heated to 120 K to reset the trapped magnetic field within the sample and then cooled in a zero field cooled regime (ZFC) to related temperature values. At these temperatures, magnetization was measured after the samples were equilibrated with a sensitivity of 0.05 K. The magnetic field was applied parallel to the *c*-axis (perpendicular to the pressing surface).

Critical current densities (J_c) and activation energies of the samples were calculated from the experimental results. The J_c was calculated using the Bean model, which is given in equation (1), and the activation energy was calculated using the Arrhenius activation energy equation given in equation (2).

$$J_c = \frac{20\Delta M}{a(1 - a/3b)} \tag{1}$$

where ΔM is the width of the magnetization curve in emu.cm^{-3}, a and b ($a < b$) are the dimensions of the sample in centimetre.

$$\rho = \rho_0 \exp\left(-\frac{U}{k_B T}\right) \tag{2}$$

where U is the magnetic field and temperature-dependent activation energy, ρ the resistivity, ρ_0 the maximum resistivity, T the temperature and k_B the Boltzmann constant [18].

3. Results and discussion

The differential thermal analysis (DTA) conducted on the melted and ground powder to investigate their influence on the peritectic temperature and the result is shown in

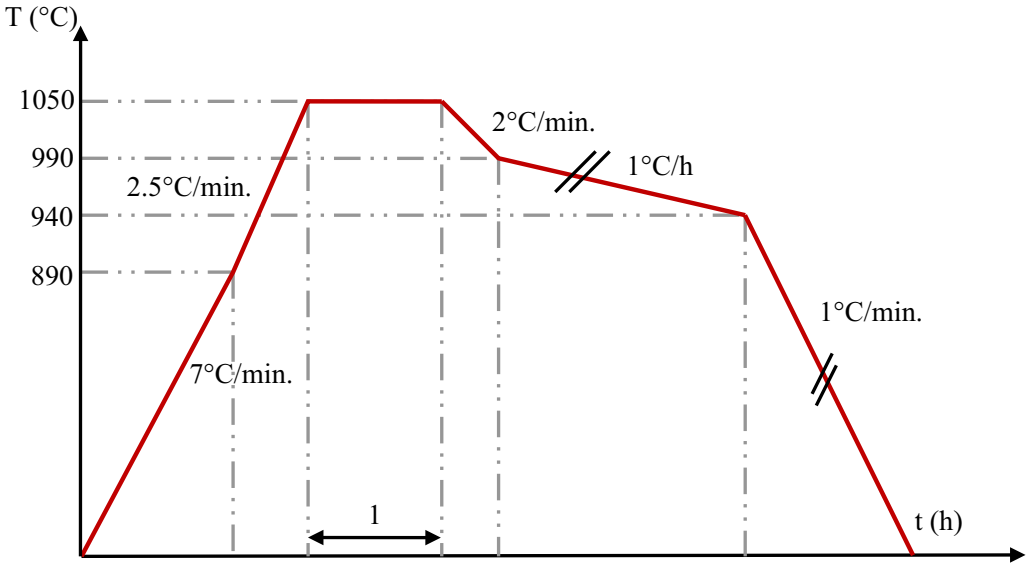

Figure 2. The thermal diagram was used for the crystal growth procedure of the Y358 samples.

figure 3. Several endothermic reaction peaks started at 920°C and an exothermic peak at about 300°C was observed. The exothermic reaction means absorption of oxygen, whereas the endothermic reaction means melting. In addition, it is seen that the powder mixture melts completely at about 1040°C. As these results are compared with the Y123 phase, it shows that the melting temperatures of the quickly cooled calcined powders prepared in the stoichiometric ratio of Y358 are approximately 40°C higher than that of Y123 [8,19].

X-ray diffraction patterns of the Y358-a, Y358-b and Y358-c samples are shown in figure 4. Superconducting phases are indicated by the presence of characteristic peaks in the XRD patterns of the samples. These characteristic peaks belong to the Y358 superconducting phase, and they are compatible with the literature [12,13,20,21]. It was observed that using the Y_2O_3 substrate for the crystal growth process did not have a significant effect on the XRD results, but only caused changes in the peak intensities.

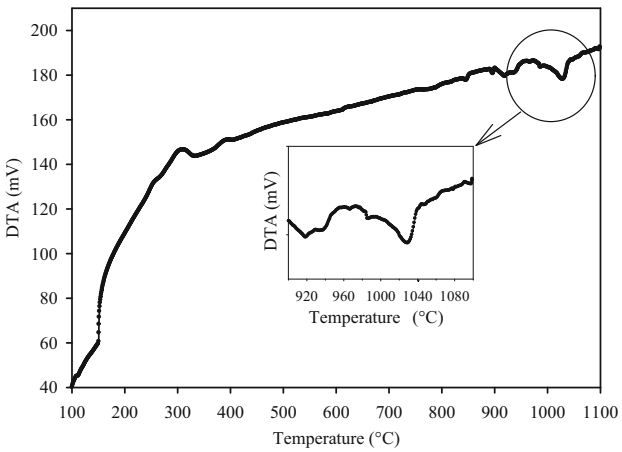

Figure 3. Differential thermal analysis (DTA) graphs of the melted Y358 powders.

Figure 5 shows polarized light optical microscope images of the samples. Among the produced samples, it is seen that the grain size of the sample with powder form Y_2O_3 substrate is relatively larger than the samples with no substrate and tablet form Y_2O_3 substrate, and the secondary phases formed at the grain boundary are less (figure 5a–c). The secondary phases accumulated at the grain boundaries cause weak link behaviour between the superconducting grains. The weak link behaviour formed between the grains affects the J_c. It is thought that the parts that appear as black regions in the grain belong to the $BaCuO_2$ phase, which has a soft structure and was cast during the polishing process. Similarly, the black regions in the matrix belong to the $BaCuO_2$ phase, which has a soft structure, and it is poured during the polishing process and creates a hole.

Figure 6a–c shows scanning electron microscope (SEM) images of Y358-a, Y358-b and Y358-c samples. In all samples, secondary phases having different shapes and sizes are seen dispersed into the superconducting phase. Besides the non-superconducting phases, holes were observed in the Y358-a and Y358-c samples. Compared to the Y358-a sample, the holes in the Y358-c sample are fewer, whereas the Y358-b sample has no holes. The gray and white phases, which are seen in figure 6b and c, were examined using the EDS analyses. The gray region indicates the superconducting phase with the ratio $Y_{3.0}Ba_{5.5}Cu_{7.7}O_{20.98}$, while the white region indicates the non-superconducting phase (figure 7). Figure 6d–f shows ImageJ analysis maps of Y358-a, Y358-b, and Y358-c samples, respectively, to determine the superconducting/non-superconducting phase fraction of the samples. As a result of the ImageJ program analysis made on the images in figure 6a–c, there is a 12% hole, 21% non-superconducting phase and 67%

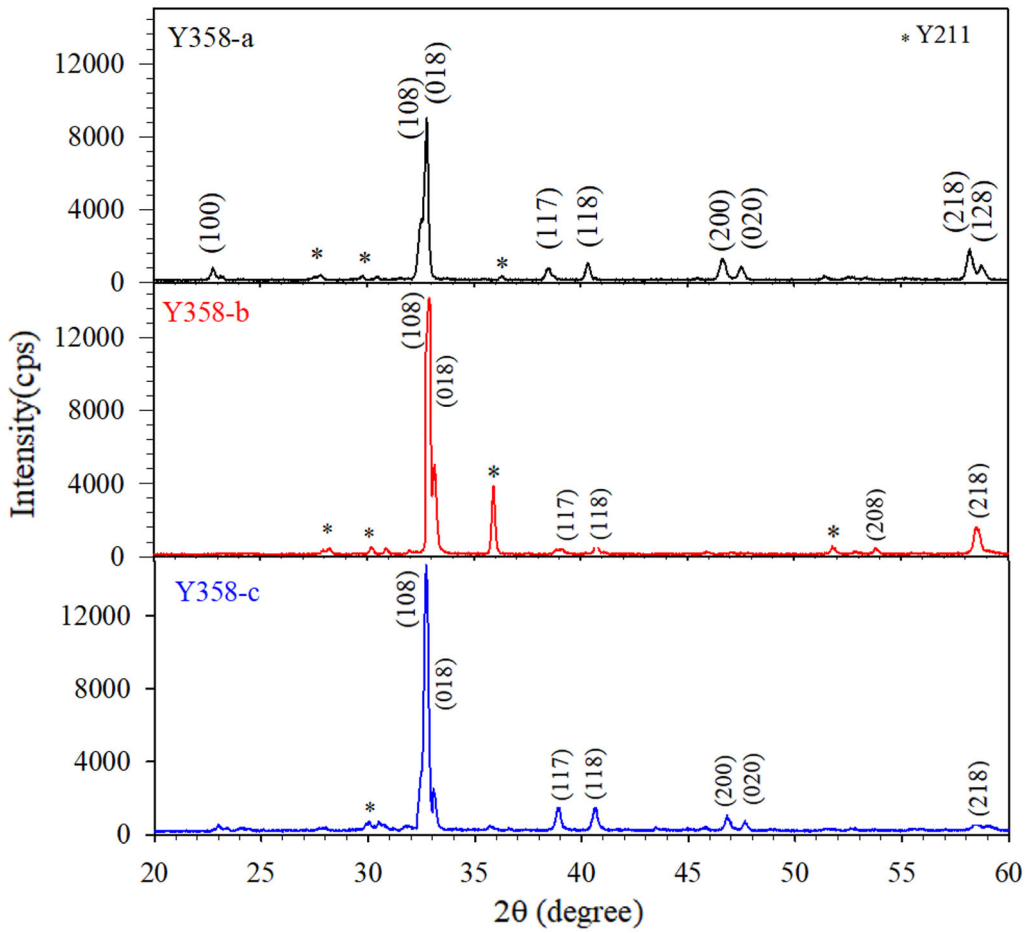

Figure 4. X-ray diffraction patterns of the Y358-a, Y358-b and Y358-c samples.

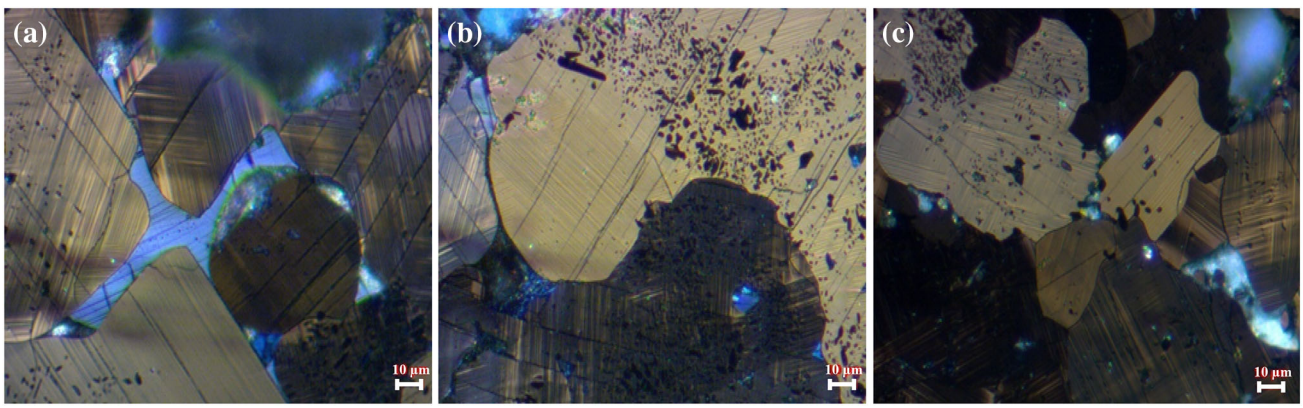

Figure 5. Polarized light optical microscope images of: (**a**) Y358-a, (**b**) Y358-b and (**c**) Y358-c samples.

superconducting phase for Y358-a sample; 24% non-superconducting phase and 76% superconducting phase for Y358-b sample; 1% hole, 28% non-superconducting phase and 71% superconducting phase for Y358-c sample.

The resistance-temperature curves for the Y358-a, Y358-b and Y358-c samples recorded under different applied magnetic fields up to 3 T are shown in figure 8. T_c^{onset} values of the samples are 96.0, 95.8 and 96.0 K and T_c^{offset} values are 95.0, 94.5 and 94.2 K for Y358-a, Y358-b and Y358-c, respectively. The transition gap from T_c^{onset} to T_c^{offset} temperature is below 2 K for all samples and it states a sharp transition. This sharp transition to superconductivity indicates single-crystal behaviour. However, the samples have a granular structure, as can be seen from the polarized optical photographs shown in figure 5. The sharp transitions of the granular samples indicate that the boundaries

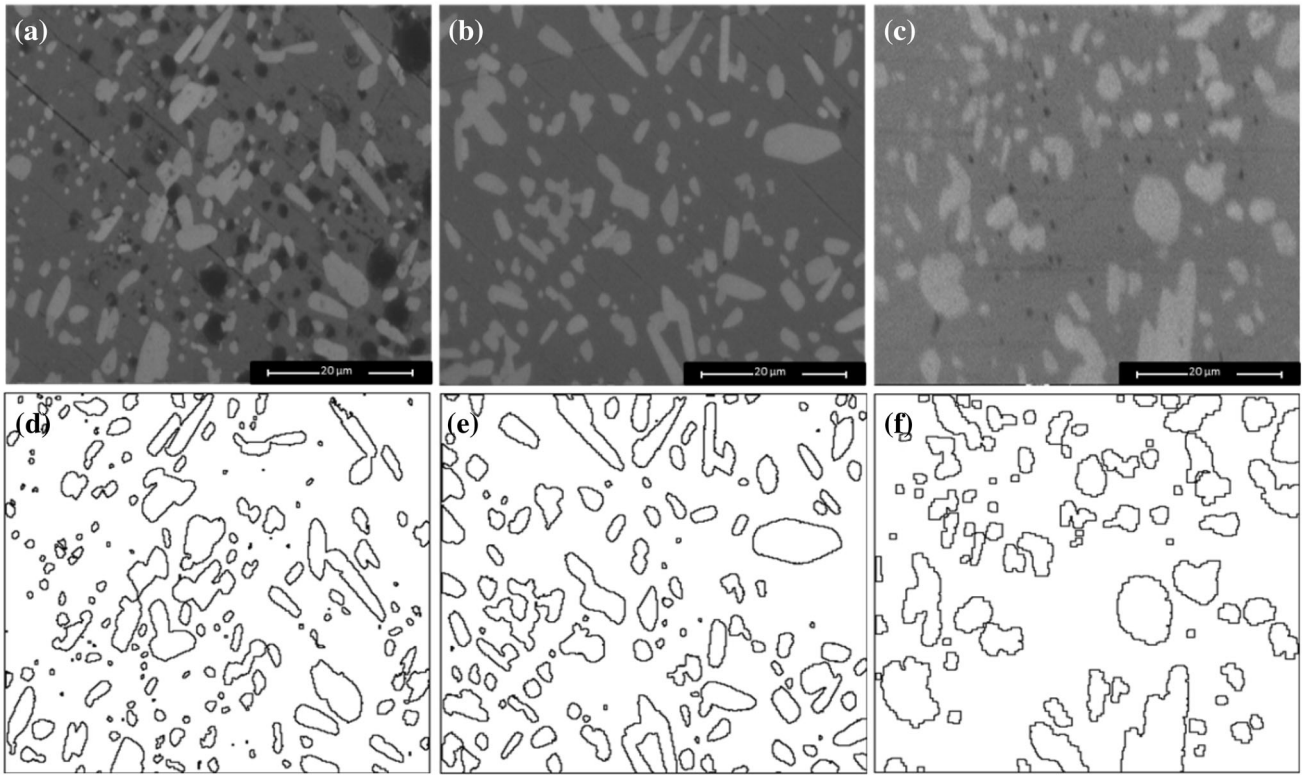

Figure 6. Scanning electron microscope (SEM) images of the (**a**) Y358-a, (**b**) Y358-b and (**c**) Y358-c samples. ImageJ analysis maps of (**d**) Y358-a, (**e**) Y358-b and (**f**) Y358-c samples.

between the grains do not exhibit weak link behaviour, and the intergranular connection is good. The superconducting transition gap also increases with an increase in the applied magnetic field, and the superconducting transition temperatures shift to lower temperatures. The increase in the transition gap was the least in Y358-b and the most in Y358-a. The width of the transition gap and the shift in resistance during the transition are proportional to the magnitude of the pinning force. When the repulsive Lorentz force exceeds the pinning force, an electric field is created and energy is lost due to electrical resistance. As the temperature decreases, the pinning force increases. For this reason, it is difficult to remove the flux lines at low temperatures and more magnetic fields are required. Thus, as the magnetic field value increases, a shift occurs in the zero-resistance temperature [22,23].

The activation energies of the samples at applied magnetic field values can be calculated directly from the slope of the $\ln(\rho/\rho_0)$ and $1/T$ linear curves according to equation (2). The variation in the calculated activation energies with the magnetic field is shown in figure 9. The activation energy to cause flux creep is highest when the magnetic field is zero, whereas it decreases with increasing magnetic field in line with the literature [24]. Since the activation energy is the energy that must be supplied to move the vortex, increasing the magnetic field leads to a decrease in the activation energy. Decreasing the activation energy with an increasing magnetic field causes the vortices to move easily [23,25]. As the magnetic field gradually increases, the pinning decreases and the superconductivity deteriorates. The determined activation energy values and pinning properties of the Y358-b sample in each applied magnetic field are higher than the other samples. The reason for this may be related to the distribution and abundance of non-superconducting particles acting as effective pinning centres [26]. Y_2O_3 substrate used in powder form is more effective than the other forms. These results are in agreement with the Y123 superconductors, which are fabricated by different types of Y_2O_3 buffer layers [16].

Figure 10 shows the magnetization hysteresis per unit volume of the Y358-a, Y358-b and Y358-c samples at 20 and 77 K, respectively. The magnetic field strengths of all samples are similar. The J_c value of the Y358-b sample having the largest loop wideness is expected to be the highest value, whereas the J_c value of Y358-a is expected to be the lowest value for both operated temperatures. The width of the hysteresis loop is proportional to the magnitude of the J_c. On the other hand, it is thought that the lower J_c value of Y358-a sample produced without using any substrate, compared to other samples, may be due to loss of liquid phase. As it is known, the Y_2O_3 layer helps to produce larger crystals by preventing the liquid phase from flowing during the crystal growth phase [16].

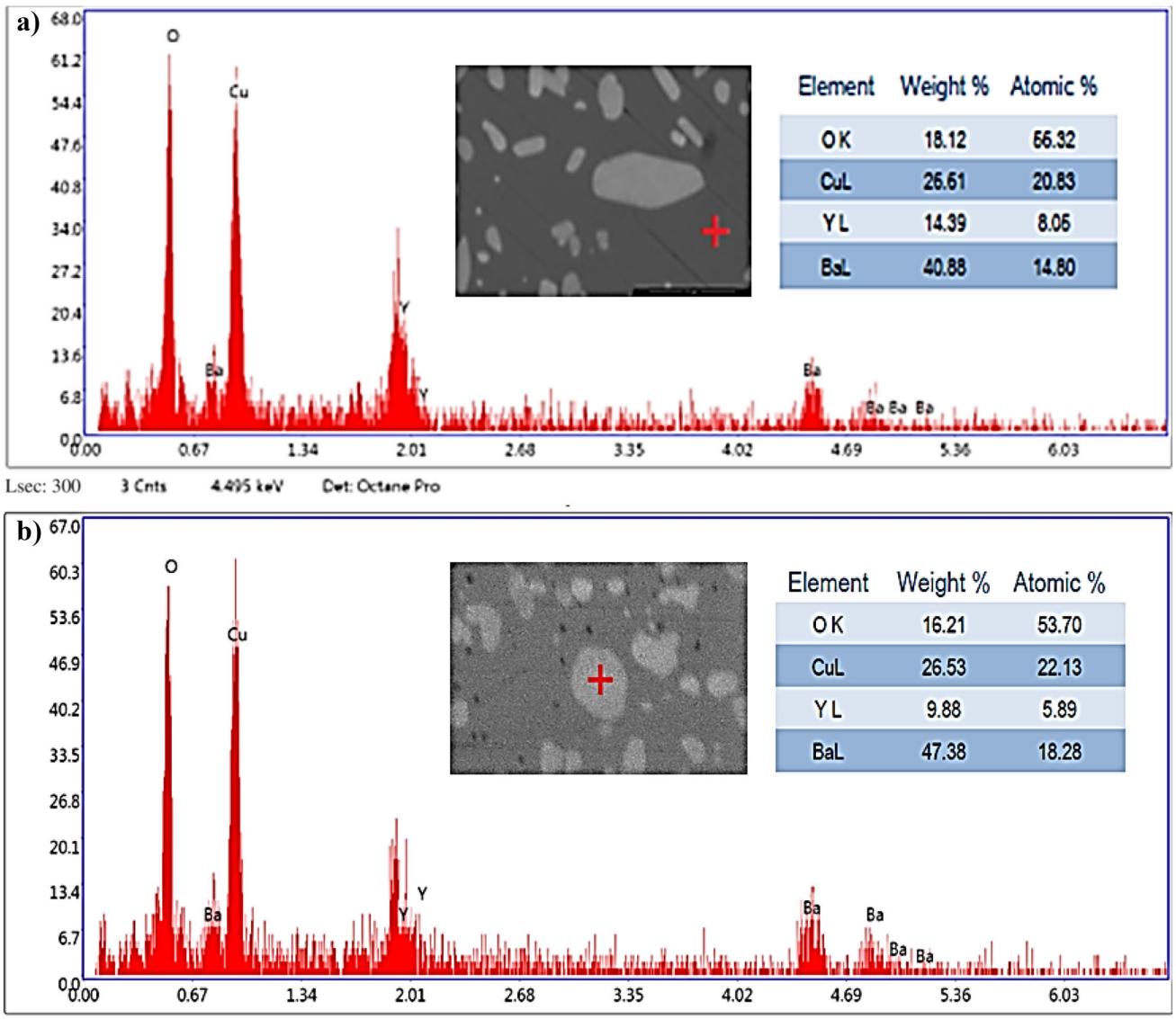

Figure 7. EDS analysis results of (**a**) the gray phase analysed from Y358-b and (**b**) the white phase analysed from Y358-c.

Figure 11 shows the magnetic field dependence of J_c calculated from the Bean critical state model for the Y358-a, Y358-b and Y358-c samples at 20 and 77 K, respectively. The J_c values decrease with the increasing applied magnetic field at a constant temperature, because of decreasing interaction between the grains at a magnetic field above a certain value. The calculated J_c values at zero magnetic field are 0.63×10^5, 1.21×10^5 and 1.0×10^5 A cm^{-2} at 20 K and 0.37×10^4, 1.2×10^4 and 1.0×10^4 A cm^{-2} at 77 K for Y358-a, Y358-b and Y358-c, respectively. It is clearly observed that the highest J_c belongs to Y358-b. As seen in the polarized optical microscope images and SEM micrographs, the Y358-b sample has a larger grain size than the other samples and has no holes in the structure. Grain boundaries and holes cause current interruption, resulting in lower J_c. In addition, it is well known that the smaller size and homogeneous distribution of the non-superconducting particles, which are dispersed in the superconducting structure and act as a strong pinning centre, play a positive role in increasing the J_c value [27].

4. Conclusion

$Y_3Ba_5Cu_8O_{18}$ (Y358) superconductors were fabricated by the Melting–Powder–Melting–Growing (MPMG) method. Two samples were produced by using Y_2O_3 substrate in powder and tablet form, and a sample was produced on an Al_2O_3 plate without using any substrate. Placing the Y_2O_3 substrate under the sample during the crystal growth process causes a decrease in the secondary phases formed at the grain boundaries and also supports the formation of larger-sized grains. Similarly, it was observed that the holes in the

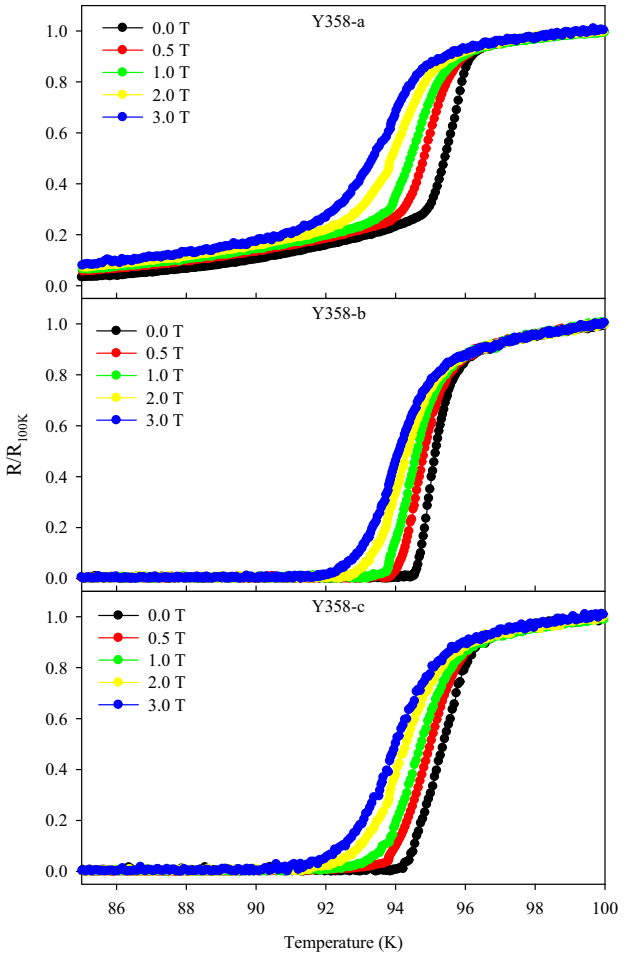

Figure 8. Resistance-temperature curves for the Y358-a, Y358-b and Y358-c samples under different applied magnetic fields up to 3 T.

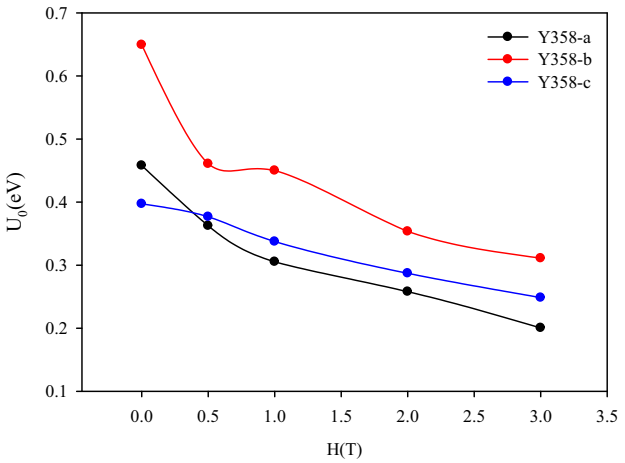

Figure 9. The variation of the calculated activation energies with the applied magnetic field of the Y358-a, Y358-b and Y358-c samples.

structure decreased. It was also seen that it was better to use the Y_2O_3 substrate in powder form as in the Y123 superconductor, because the highest activation energy and the highest critical current density values which are calculated in zero magnetic field belong to the sample produced with powdered Y_2O_3 substrate. The Y_2O_3 substrate used in powder form is more effective than the other forms in growing larger superconducting grains in both Y358 and Y123 superconductor families.

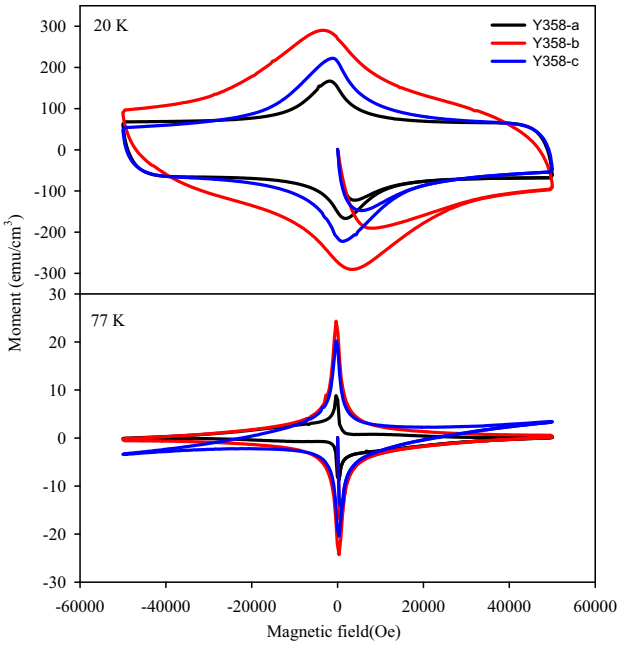

Figure 10. Magnetization hysteresis curves of the Y358-a, Y358-b and Y358-c samples at 20 and 77 K.

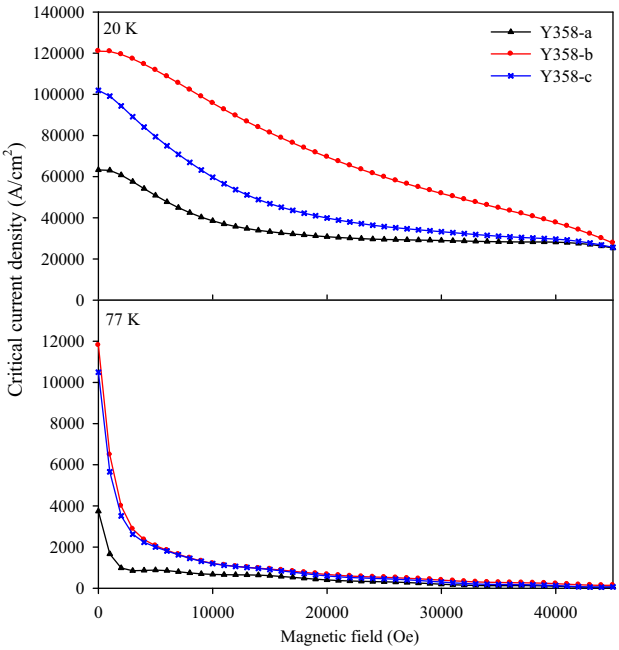

Figure 11. Magnetic field dependence of critical current density, J_c, calculated from the Bean critical state model at 20 and 77 K.

Acknowledgement

This work was supported by the Turkish Science and Technology Council-TUBITAK under Project Number 117F484.

References

[1] Hull J R 2000 *Supercond. Sci. Technol.* **13** R1
[2] Fujimoto H 2000 *Supercond. Sci. Technol.* **13** 827
[3] Murakami M, Sakai N, Higuchi T and Yoo S I 1996 *Supercond. Sci. Technol.* **9** 1015
[4] Nariki S, Sakai N and Murakami M 2002 *Supercond. Sci. Technol.* **15** 648
[5] Ikuta H, Mase A, Mizutani U, Yanagi Y, Yoshikawa M, Itoh Y *et al* 1999 *IEEE Trans. Appl. Supercond.* **9** 2219
[6] Tomita M and Murakami M 2003 *Nature* **421** 517
[7] Namburi D K, Shi Y and Cardwell D A 2021 *Supercond. Sci. Technol.* **34** 053002
[8] Murakami M 1992 *Supercond. Sci. Technol.* **5** 185
[9] Murakami M 2001 *Physica C* **357–360** 751
[10] Bondarenko S I, Koverya V P, Krevsun A V and Link S I 2017 *Low Temp. Phys.* **43** 1125
[11] Bernstein P and Noudem J 2020 *Supercond. Sci. Technol.* **33** 1
[12] Aliabadi A, Farshchi Y A and Akhavan M 2009 *Physica C* **469** 2012
[13] Gholipour S, Daadmehr V, Rezakhani A T, Khosroabadi H, Shahbaz Tehrani F and Hosseini Akbarnejad R 2012 *J. Supercond. Nov. Magn.* **25** 2253
[14] Bolat S and Kutuk S 2012 *J. Supercond. Nov. Magn.* **25** 731
[15] Basoğlu M, Düzgün I and Öztürk A 2021 *J. Supercond. Nov. Magn.* **34** 1077
[16] Aydıner A, Çakır B, Seki H and Başoğlu M 2011 *J. Supercond. Nov. Magn.* **24** 1397
[17] Çakır B and Aydıner A 2011 *J. Supercond. Nov. Magn.* **24** 1577
[18] Zou X W, Wang Z H, Chen J L and Zhang H 2001 *Physica C* **356** 31
[19] Licci F, Tissot P and Scheel H J 1989 *J. Less Common Metals* **150** 201
[20] Udomsamuthirun P, Kruaehong T, Nikamjon T and Ratreng S 2010 *J. Supercond. Nov. Magn.* **23** 1377
[21] Slimani Y, Hannachi E, Ben Salem M K, Ben Azzouz F and Ben Salem M 2018 *Appl. Phys. A* **124** 1
[22] Yazıcı D, Erdem M and Özçelik B 2012 *J. Supercond. Nov. Magn.* **25** 725
[23] Abou El Hassan A, Taoufik A, Labrag A, Bghour M, El Hamidi H and Ait Ahmed Y 2021 *E3S Web of Conferences* **229** 01014
[24] Kutuk S, Bolat S, Terzioglu C and Altintas S P 2015 *J. Alloy. Compd.* **650** 159
[25] Labrag A, Bghour M, Abou El Hassan A, El Hamidi H, Taoufik A and Laasri S 2020 *Eur. Phys. J. Appl. Phys.* **92** 20601
[26] Aliabadi A, Akhavan-Farshchi Y and Akhavan M 2013 *J. Supercond. Nov. Magn.* **27** 741
[27] Naik S P K, Miryala M, Koblischka M R, Koblischka-Veneva A, Oka T and Murakami M 2020 *ACS Omega* **5** 6250